[4]T. F. Gallagher, L. M. Humphrey, W. E. Cooke, R. M. Hill, and S. A. Edelstein, Phys. Rev. A 16, 1098 (1977); T. W. Ducas, M. G. Littman, R. R. Freeman, and D. Kleppner, Phys. Rev. Lett. 35, 366 (1975).

[5]M. G. Littman, M. L. Zimmerman, and D. Kleppner, Phys. Rev. Lett. 37, 46 (1976); M. G. Littman, Ph.D. thesis, Massachusetts Institute of Technology, 1976 (unpublished).

[6]M. G. Littman, M. M. Kash, and D. Kleppner, Phys. Rev. Lett. 41, 103 (1978).

[7]See, for example, D. S. Bailey, J. R. Hiskes, and A. C. Riviere, Nucl. Fusion 5, 41 (1965).

[8]R. R. Freeman and D. Kleppner, Phys. Rev. A 14, 1614 (1976).

[9]W. R. S. Garton and F. S. Tomkins, Astrophys. J. 158, 839 (1969); R. J. Fonck, D. H. Tracy, D. C. Wright, and F. S. Tomkins, Phys. Rev. Lett. 40, 1366 (1978); N. P. Economou, R. R. Freeman, and P. F. Liao, Phys. Rev. A (to be published).

[10]For a discussion of quantization of one-dimensional electric fields see R. F. O'Connell, Phys. Rev. A 17, 1984 (1978), and Phys. Lett. 60A, 481 (1977).

[11]R. R. Freeman and G. C. Bjorklund, Phys. Rev. Lett. 40, 118 (1978).

Pulsed-X-Ray Shadowgraphy of Dense, Cool, Laser-Imploded Plasma

M. H. Key,[a] C. L. S. Lewis, J. G. Lunney, and A. Moore
Queen's University, Belfast, Scotland

and

T. A. Hall
University of Essex, Colchester, United Kingdom

and

R. G. Evans
Science Research Council Rutherford Laboratory, Chilton, Didcot, Oxfordshire OX11 0QX, United Kingdom

(Received 31 July 1978)

Laser implosion of 87-bar neon-filled glass microballoon targets produces a dense, cool plasma whose development in time and space is recorded by pulsed-x-ray shadowgraphy with soft x rays from a separate laser-produced plasma. Compressed densities of 4 g cm^{-3} are estimated from the data by comparison with numerical simulations of the implosion.

A new approach to space- and time-resolved diagnosis of dense plasmas produced by laser-driven implosions has been developed. Pulsed-x-ray shadowgraphy, with a separate laser-produced plasma as the x-ray source, has given images of plasmas of high density but low temperature which cannot be diagnosed by the more usual methods based on the emission of x rays and fusion-reaction particles.

In this initial investigation a target design was chosen to create plasmas of density >1 g cm^{-3} and temperature <100 eV, and to implode in 500 ps when driven by a 4-J, 100-ps, Nd-glass laser pulse. The targets were glass microballoons filled with neon at 87 bar, typically of 66 μm diam and of 1.3 μm glass shell thickness. They were irradiated by two beams with $f/1$ lens focusing. A laser pulse of 5 J in 100 ps, and variable delay with respect to the beams irradiating the microballoon, was directed through one of the lenses and focused on a brass (Cu + Zn) target as

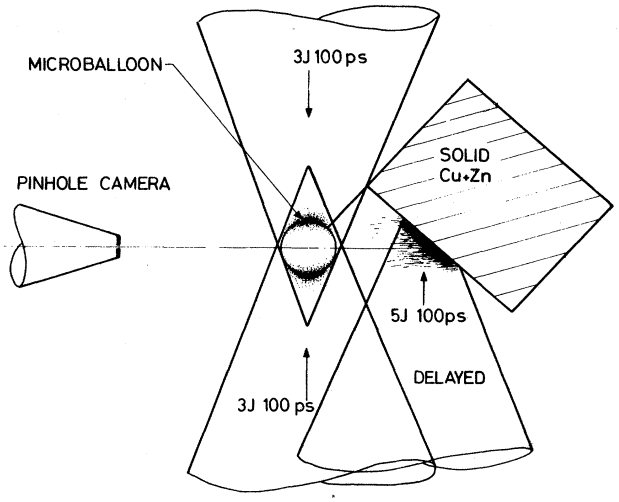

FIG. 1. Experimental configuration for pulsed-x-ray shadowgraphy. The 66-μm-diam microballoon, its support fiber, and the plasma on the brass target are drawn in correct relative scale. The schematic pinhole was 2.5 cm from the microballoon.

shown in Fig. 1. There it produced a plasma of 200 μm diam which emitted a pulse of soft x rays whose 100-ps duration was estimated from x-ray streak-camera data (1) whose spectrum is discussed below.

This plasma was imaged on Kodirex film by an x-ray pinhole camera with a 12-μm pinhole, 4× magnification, 2.5-cm pinhole-to-plasma distance, and a Be filter with e^{-1} transmission at 1.8 keV photon energy. The microballoon was positioned on the axis of observation of the pinhole camera so that the image of the emission from the brass-target plasma had superimposed on it a shadowgraph of the absorbing regions of the microballoon target. Figure 2 shows a series of such images in which the delay between the irradiation of the microballoon and the brass target has been varied. The two beams irradiating the microballoon were focused for maximum uniformity of illumination with the marginal rays tangential to the sphere as shown in Fig. 1. Separate shots were used to record the emission from each of the two plasmas alone. These showed that the brass-target plasma image was 10 times more intense than that of the microballoon, which was ringlike with no observable central emission peak.

It is seen in Fig. 2 that the imploding plasma is spherical and that its diameter decreases to a minimum at 450- to 570-ps delay and then expands again. In the early stages (250- and 350-ps delay) there is a ring structure of maximum absorption with an increase in transmission at the center indicating a dense shell of imploding material. It was concluded from the observations above that the finite intensity in the zones of maximum absorption in Fig. 2 was due to the relatively weak emission from the microballoon target itself.

The densitometer traces of the shadowgraph images were transformed to intensity profiles which were, to a sufficient approximation for the conditions in Fig. 1, $I_b(x)T_i(x)+I_i(x)$, where $I_b(x)$ and $I_i(x)$ are the intensity profiles of the background and implosion plasmas individually and $T_i(x)$ is the transmission profile of the implosion plasma. In analyzing this experiment it was assumed that at the point of maximum absorption $I_b(x)T_i(x)$ was negligible so that the microballoon emission profile $I_i'(x)$ measured on a different shot could be normalized, centered on the absorption feature, and subtracted yielding $I_b(x)T_i(x)$. This normalization was retrospectively justified as discussed below. Similarly the separately measured profile $I_b'(x)$ was centered and normalized relative to $I_b(x)T_i(x)$ in the outer region where $T_i(x)\to 1$, allowing computation of $T_i(x)$ from the ratio of the two profiles. Plots of opacity, $\tau(x)=-\ln T(x)$, derived in this way are shown in Figs. 3(a) and 3(b). The implosion was also modeled theoretically using a one-dimensional fluid code MEDUSA whose main features are described elsewhere.[1,2] The code results indicated implosion core temperatures of 50 to 100 eV and density 0.5 to 1 g cm^{-3}. The calculations also simulated the shadowgraph experiment by computing $\tau(x)$. It was assumed that, to sufficient accuracy, absorption of x rays in the experimental energy range could be represented by photoionization of K-shell electrons of oxygen and neon in the glass and gas, respectively, and that the ion species present in the dense regions of the implosion would have two K electrons. The absorption coefficient $K(\nu)$ was obtained from the Kirchhoff-Planck relationship and the intensity of free-bound emission in a plasma of two electron ions[3] and can be written as

$$K(\nu)=(4.1\times 10^{-16})X^2n/\nu^3 \text{ cm}^{-1}$$

for ionization potential X and photon energy ν in

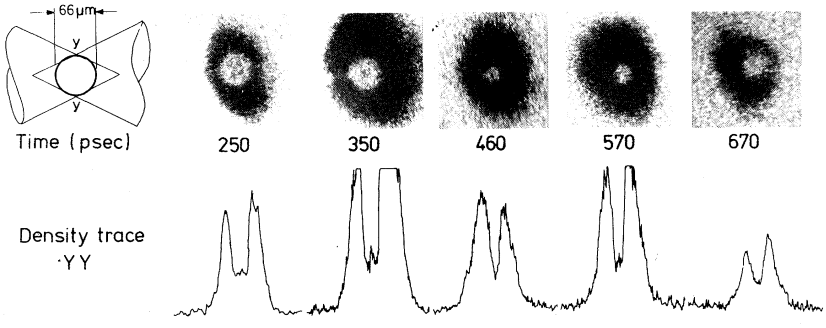

FIG. 2. A series of pulse–x-ray shadowgraph images and their densitometer traces for various delays from the laser-pulse peak.

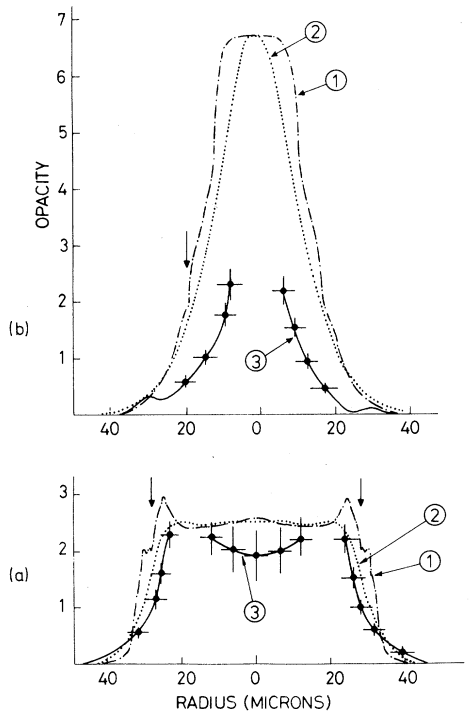

FIG. 3. Opacity plots for (a) analysis at 250 ps delay; (b) analysis at 460 ps delay. (1) The computed opacity profile; (2) the computed profile transformed by the finite resolution of the pinhole camera; (3) the experimental capacity profile $\tau(x)$. Vertical arrows indicate the gas/glass boundary.

electron volts and ion number density n.

The spectrum $I(\nu)$ from the brass-target plasma transmitted by the Be filter was recorded with a calibrated x-ray spectrometer[1] and found to be mainly due to Cu XX and Zn XXI line radiation in an 0.5-keV band centered at 1.5 keV. It was used in calculating $\tau(x)$ since

$$\tau(x) = \ln\left|\int I(\nu)\, T(x\nu)\, d\nu / \int I(\nu)\, d\nu\right| .$$

The computed opacity profiles illustrated in Figs. 3(a) and 3(b) have peak values of opacity large enough to justify the earlier assumption of no observable transmission in the region of greatest opacity. They also show that the absorption due to the glass is the dominant factor with the peak of the opacity profiles occurring near the gas/glass interface. The computer profiles were transformed to a form consistent with imaging by the pinhole camera by assuming circular symmetry of the source and a geometrically ideal rectangular intensity profile for a point source imaged by the pinhole. This reduced the apparent size of the zone of high opacity as illustrated in Fig. 3.

A reasonably good agreement was obtained between the experimental and predicted forms of the opacity profile at the earliest recorded stage of the implosion where the main feature is the imploding glass shell; see Fig. 3(a). The experimental profile is indeterminate at the point of maximum opacity because of the normalization assumption. The maximum meaningful value of the opacity was found to be 2 to 3 by analyzing "best-estimate" and "uncertainty-range" smoothed profiles drawn through the film grain noise of the densitometer traces. The calculated profile at peak compression shown in Fig. 3(b) is not in such good agreement with the experimental data which indicate a smaller region of high opacity. This suggests either that a smaller fraction of the target mass was in the implosion core or that the compressed density was higher than that calculated. (A poorer effective spatial resolution of the pinhole camera, >30 μm, would also account for this but is inconsistent with the pinhole size and the resolution obtained in test images of unirradiated microballoons.)

One reason for the compressed density to be higher than the calculated value is that radiation cooling and ionization energy, which both reduce the temperature and thus the pressure opposing the implosion, were not treated in the code. The simulation results are sensitive to such effects. For example, representation of radiation cooling as optically thin bremsstrahlung radiation resulted in a twentyfold increase in compressed density. A better calculation including self-absorption would evidently give an intermediate result.

If it is assumed that increased density explains the above discrepancy between observation and calculation, then the core density can be roughly estimated by a scaling argument. The ratio of observed to computed core diameter in Fig. 3(b) is 0.6 ± 0.1 at $\tau = 2$. The computed volumetric compression ratio in the core was 10 and it may therefore be inferred that this was increased to 50 ± 25 in the experiment so that the experimental core density was 4 ± 2 g cm^{-3}.

While this is of some interest as a high compressed density it is perhaps more significant that the experiment has demonstrated the potential of x-ray shadowgraphy in the diagnosis of dense implosions. The technique should be of particular value in future studies of ablatively driven implosions.

The authors acknowledge the contribution of P. T. Rumsby in providing the targets for the experiment. The work was carried out at the Cen-

tral Laser Facility, Rutherford Laboratory, England.

[a]Present address: Science Research Council Rutherford Laboratory, Chilton, Oxon OX11 0QX, England.

[1]M. H. Key *et al.*, Science Research Council Rutherford Laboratory Central Laser Facility Report No. LD/78/01, 1978 (unpublished).

[2]J. P. Christiansen, D. E. T. F. Ashby, and K. V. Roberts, Compu. Phys. Commun. 7, 271 (1974).

[3]G. Elwert, Z. Naturforsch. 9A, 637 (1954).

Spectrum Cascade by Mode Coupling in Drift-Wave Turbulence

Akira Hasegawa
Bell Laboratories, Murray Hill, New Jersey 07974

and

Yuji Kodama
Department of Mathematics, Clarkson College, Potsdam, New York 13676

(Received 14 June 1978)

The spectrum cascade by mode coupling in drift-wave turbulence occurs to larger and smaller values of $|\vec{k}|$ rather than toward lower frequencies. This leads to the dual cascade process; energy cascades to smaller k while enstrophy (square of the vorticity) cascades to larger k, analogous to two-dimensional hydrodynamic turbulence. However, the speed of energy condensation to $k=0$ is much slower than in the hydrodynamic case.

In this Letter, we show that the spectrum cascade by mode coupling in drift-wave turbulence occurs to longer and shorter wavelengths, and that it leads to the dual cascade process where the energy cascades to smaller k, while the entropy cascades to larger k, analogous to two-dimensional hydrodynamic turbulence.[1] This result originates from an intrinsic property of the drift wave in which the linear frequency and the amplitude can be small parameters of the same magnitude.

For wave-wave interactions in drift-wave turbulence the largest coupling occurs through the $\vec{E}\times\vec{B}$ nonlinearity. This allows us to ignore the parallel ion inertia. The best way of deriving the nonlinear equation in such a case is to use the vortex equation for the ion dynamics.[2] If we make the assumption of cold ions, the equation for the vorticity $\Omega=(\nabla_\perp\times\vec{v}_\perp)\cdot\hat{z}$ can be derived by taking the curl of the ion equation of motion and by using $\nabla_\perp\cdot\vec{v}_\perp=-d\ln n/dt$:

$$\frac{d}{dt}\ln\left(\frac{\omega_{ci}+\Omega}{n}\right)=0, \tag{1}$$

where ω_{ci} is the ion cyclotron frequency, n is the number density, and $\vec{v}_\perp$ is the ion velocity in the direction perpendicular to the ambient magnetic field $B_0\hat{z}$. The total derivative includes the convective derivative,

$$\frac{d}{dt}=\frac{\partial}{\partial t}+(\vec{v}_\perp\cdot\nabla), \tag{2}$$

where the leading term in $\vec{v}_\perp$ is given by the $\vec{E}\times\vec{B}$ drift,

$$\vec{v}_\perp=-\nabla\varphi\times\hat{z}/B_0. \tag{3}$$

Here, φ is the electrostatic potential of the drift wave. The number density is given by the electron density as a result of the quasineutrality condition:

$$n=n_0(\vec{x})(1+e\varphi/T_e), \tag{4}$$

where T_e is the electron temperature and the contribution from the Landau pole due to the electron parallel motion is ignored by assuming a saturated state. The vorticity Ω is obtained from Eq. (3),

$$\Omega=(\nabla^2\varphi)/B_0. \tag{5}$$

If we substitute Eqs. (4) and (5) into (1), we obtain the following exact simple nonlinear equation for the drift-wave turbulence[3]:

$$\partial(\nabla^2\varphi-\varphi)/\partial t+[(\nabla\varphi\times\hat{z})\cdot\nabla](\ln n_0-\nabla^2\varphi)=0, \tag{6}$$

where the time and space coordinates are normalized by ω_{ci}^{-1} and $\rho_s=(T_e/m_i)^{1/2}/\omega_{ci}$ and the potential φ by T_e/e.

To find the direction of the spectrum cascade in Eq. (6), we consider three waves with the wave numbers $\vec{k}_1$, $\vec{k}_2$, and $\vec{k}_3$ such that $\vec{k}_1+\vec{k}_2+\vec{k}_3=0$.[4] If we write

$$\varphi(\vec{x},t)=\varphi_{\vec{k}}(t)\exp(i\vec{k}\cdot\vec{x})+\text{c.c.},$$

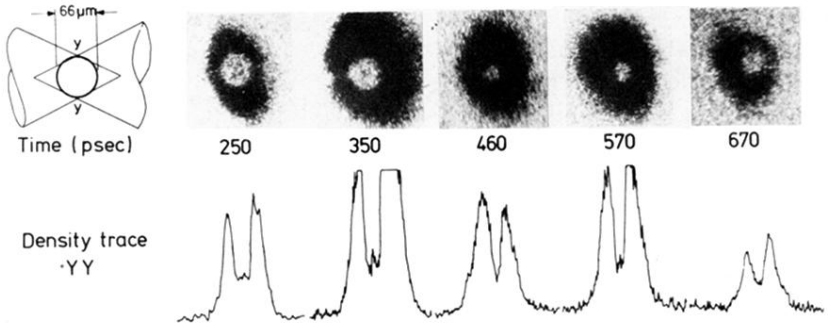

FIG. 2. A series of pulse–x-ray shadowgraph images and their densitometer traces for various delays from the laser-pulse peak.